Super Resolution Ultrasound Imaging: investigating the effect of processing parameters and flow orientation on image quality

Andrej Shoykhet

***Abstract*—Super Resolution (SR) Ultrasound (US) imaging combines high spatial resolution with high penetration depth imaging to an extent that is currently not available by other *in vivo* imaging modalities. SRUS relies on detection, localization and tracking of single microbubbles (MBs) in blood vasculatrue. This study focuses on how to set SRUS processing parameters to obtain a SR image and on the effect of flow direction on the resolution. To analyze the effect of processing parameters, acquisitions of chicken embryos and of *ex vivo* rabbit kidneys were performed and SRUS processing was done with different parameter settings. The effect of flow direction was measured using a custom-made phantom with two crossing tubes and using flow simulations of that phantom. Image filtering and the choice of sufficiently small pixels in the B-Mode image reconstruction showed to have the most effect on SRUS images. SRUS images were shown to be independent of flow direction whereas the flow direction affected the resolution of power Doppler images. This study provides a guideline for setting SRUS processing parameters.**

I. Introduction

In modern healthcare, vascular imaging is crucial for the diagnosis of many diseases. Often a trade-off has to be made between imaging depth and resolution [1]. While optical methods are limited to superficial imaging, conventional Ultrasound (US), MRI, and PET give a limited resolution inside tissue. Super Resolution (SR)US might fill the gap by providing a high-resolution (in the rage of μm) vascular imaging modality with significant penetration depth (multiple cm) [1]. To understand how SR is achieved it is important to understand why resolution is limited with conventional US. In 1873, the resolution limit for light microscopy was described by Ernest Abbe [2]. Two point-sources can only be resolved if their distance is not less than about 1/2 of the imaging wavelength. Thus, the highest possible resolution is dependent on the wavelength of light. For a higher resolution shorter wavelengths have to be used (as done in X-Ray microscopy). These limits can be transferred to US imaging. To get a higher resolution in US, one can use higher US frequencies, meaning shorter US wavelengths. However, the drawback of short wavelength US imaging is a high attenuation of the sound waves in the tissue, resulting in a low penetration depth. The resolution limit for optical and ultrasonic systems seemed to be insurmountable. However, at the beginning of this century, new microscopy methods were developed that surpassed the diffraction limits described by Abbe. In 2014, the Nobel Prize in Chemistry was awarded to Eric Beizing, Stefan W.Hell, and Wiliam E. Moerener for the development of methods that can be summarized under the name "Nanomicroscopy" or "Super-Resolution Microscopy". Some of these methods (location microscopy) rely on imaging sparsely distributed fluorophores. The sparse distribution and the knowledge of the Point Spread Function (PSF) of the fluorophores allows localization with a precision that is higher than the resolution limit described by Abbe [3]. The concept of Super-resolution Microscopy can be transferred to US imaging. In 2015 Errico et al. proved the possibility of SRUS imaging [4]. Instead of fluorophores, microbubbles (MBs) which are known from Contrast Enhanced Ultrasound Imaging (CEUS) are used as point scatterers. Knowing the PSF of MBs in a US image, MB localization can be performed at a sub-diffraction limit precision. With high framerate US imaging, the path of MBs in vessels can be tracked allowing the reconstruction of the (micro-)vasculature. SRUS imaging allows imaging deep inside tissue, with a resolution of up to 10 μm at a transmit frequency of (15 MHz), which means a resolution of 10 times higher than the transmitted wavelength [5].

While general resolution limits of SRUS are explored [6], there is little evidence about the influence of flow direction on SRUS and about disturbances due to close-by vessels. Furthermore, on the path from the received echos by the transducer to a final SRUS image many parameters have to be chosen correctly. In other publications, separate SRUS processing steps were investigated. Heiles et al. [7] and Song et al. [8] compared different localization methods for MBs. Huang et al. [9] showed how to improve image quality by modifying Singular Value Decomposition (SVD) filtering or by filtering MBs by their speed.

The aim of this work is to investigate how different flow orientations and different parameters throughout several processing steps influence the final image. For this purpose, acquisitions were performed on *in vivo* chicken embryos, *ex vivo* rabbit kidneys, and a custom-made flow phantom which was also simulated. SRUS processing was performed on these acquisitions with different parameter settings.

II. Materials and Methods

A. Imaging System

All US acquisitions were performed on a Verasonics Vantage System (Verasonics Inc., Kirkland, WA, USA) with an L11-5v (Verasonics Inc., Kirkland, WA, USA) transducer using a center frequency of 7.6 MHz for transmit pulses. For high framerate B-Mode acquisitions 5 angle (-6°, -3°, 0°, 3°,

6°) compounding plane wave acquisitions were used with a post-compounding framerate of 500 Hz. Single-cycle transmit pulses were used for all acquisitions. During acquisitions, only the received RF data was saved. Image reconstruction was performed off line. During all acquisitions, the transducer was mounted on a motorized platform, enabling precise translation in three directions.

B. Phantom

A custom-made flow phantom was used to investigate the effect of flow orientation on the image quality. The cylindrical polyacrylamide (PAA) phantom had two wall-less tubes with a diameter of 200 μm that were parallel to the basis of the cylinder. The phantom was prepared using 450 mL of Acrylamide/Bis-acrylamide solution (29/1, 40% solution, Sigma-Aldrich), 1350 mL degassed water, 2,7 mL N,N,N,N'-Tetramethyl ethylenediamine (TEMED, 99%, Sigma-Aldrich), and 2,7 g Ammonium persulfate (APS, 99%, Sigma-Aldrich). The tubes were positioned to have the closest point to each other at the center of the cylinder with a projected angle of intersection of 30° and a distance from one another in the range of 1 mm at the closest point. The inner diameter of the phantom was 17 cm (resulting in a required imaging depth of 8.5 cm to have the crossing in the field of view) (Supplementary Figure 1).

C. Microbubbles

SonoVue MBs (Bracco Imaging S.p.A., Milan Italy) were used in all experiments. The MB suspension was prepared according to the manufacturer's instructions resulting in an initial MB concentration of $2 * 10^8 \frac{MB}{ml}$.

D. Chicken Embryos

Fertilized eggs were collected from a chicken breeding factory. The eggs were placed for three days in an incubator at 37°C. On embryonic day 3 the eggshell was broken and the contents (embryo, yolk, egg white, and chorioallantoic membrane (CAM)) were placed into a sterilized modified weighing boat. In the weighing boat, one side was cut away and replaced with a vertical Mylar wall (thickness 46 μm), that was glued to the weighing boat using silicone. The weighing boats with the embryos were placed back into an incubator. For this study US acquisition of one chicken embryo was used. The acquisition was performed on embryonic day 12. The Mylar wall allowed US imaging of the embryo from the side as well as moving the transducer up- and downwards without moving the embryo (Supplementary Figures 4 and 5). The eggs were incubated and opened at the nephrology department of the UMC Utrecht.

E. Rabbit Kidney

A *post mortem* rabbit was collected from a butcher and the rabbit kidneys were stored for four days in a fridge before reperfusion and performing US acquisitions.

F. Post-processing

The general steps of SRUS are image filtering, MB detection, localization, and tracking. The SRUS processing scripts used in this study were adapted from the publications by Heiles et al. [7] and Denis et al. [10]. Some additional steps were added which were introduced by Song et al. [11] and Huang et al. [9].

1) B-Mode image reconstruction: The image reconstruction from RF to intensity (IQ) data (delay and sum beamforming and spatial compounding) was performed with the built-in Verasonics reconstruction software.

2) Filtering: To suppress tissue signal and for optional MB speed filtering three different SVD-based filtering approaches were tested which will be described in more detail in section II-G2. Additionally, noise equalization was performed by multiplying the SVD-filtered data with a 1D noise profile as described by Huang et al. [9]. The whole filtering step was skipped for simulation data since no stationary tissue was present in the simulations and the noise level was uniform across the image.

3) Localization: On the filtered images MBs appear as bright structures. To detect these structures and to localize MBs, local maxima were detected on each frame. The localization algorithm was performed on a 5x5 pixel window around a selection of brightest local maxima using a radial symmetry algorithm [7] [12].

4) Tracking: After localizing potential MBs on separate frames, MBs were tracked across frames. For tracking, the simpletracker (https://github.com/tinevez/simpletracker) was used, which is based on the Hungarian algorithm. The detected tracks were then drawn into a high-resolution image (often called track accumulation). The pixel size of the SRUS images was five times smaller than the wavelength of the transmitted ultrasound pulses.

G. Processing Parameters

The effect of the following parameters was investigated during the post-processing. One set of parameters was chosen as a reference before always changing one parameter at a time. The parameter settings are summarized in Table I.

1) B-Mode image reconstruction: Initial pixel size: The first parameter was the pixel size which was used for B-Mode image reconstruction.

2) Filtering: SVD cutoff and additional filtering: Three different SVD filter designs were tested to suppress tissue signaling while enhancing MB signaling:

a) SVD filter: An SVD filter allows to suppress tissue signal while enhancing MB signal. Here, SVD filters with a cut-off of the first 5 and the first 40 singular values were compared.

b) SVD + optional bandpass: A more advanced filtering method used in this study was described by Denis et al. [10]. For slow-moving MBs, a SVD filter with a cut-off of the first 10 singular values was combined with a Butterworth bandpass filter with cutoff frequencies of 5 and 80 Hz. For fast-moving MBs, only one SVD filter with a cutoff of the first 40 singular values was used.

TABLE I
ANALYZED PROCESSING PARAMETERS

Parameter to analyze	initial pixel size	number of expected MB	maximum linking distance in Pixel	minimum track length in pixel	Filter design
Reference	0.5x0.5 λ	200	1.5	20	SVD, cutoff 5
Initial pixel size	0.5 λ axial 1.4805λ lateral	200	1.5	20	SVD, cutoff 5
Initial pixel size	0.5 λ axial 1.4805λ lateral; interpolation to 0.5x0.5 λ	200	1.5	20	SVD, cutoff 5
SVD cutoff	0.5x0.5 λ	200	1.5	20	SVD, cutoff 40
Additional filtering	0.5x0.5 λ	200	1.5	20	SVD, cutoff 40
		400	0.8	20	SVD, cutoff 10+ band-pass
Additional filtering: cone shaped filter in fourier space	0.5x0.5 λ	200	1	20	cone filter μ=0 mm/s
			1.5	20	cone filter μ=5 mm/s
			1.5	20	cone filter μ=10 mm/s
			2	20	cone filter μ=15 mm/s
number of expected MBs	0.5x0.5 λ	500	1.5	20	SVD, cutoff 5
minimum track length	0.5x0.5 λ	200	1.5	5	SVD, cutoff 5
maximum linking distance	0.5x0.5 λ	200	4	20	SVD, cutoff 5

c) Fourier space cone filter: A filter similar to that described by Huang et al. [9] was implemented. A cone-shaped Gaussian filter was applied to the 3D Fourier transform of the intensity data. In a cylindrical coordinate system where θ is the angle from the z-axis, the intensity of the cone was described by: $I = e^{-\frac{(\theta-\mu)^2}{2*\sigma^2}}$. As described by Huang et al., signals of MBs at a certain speed are concentrated in a cone which makes each θ corresponding to a certain MB velocity. μ describes the velocity shift from 0 velocity for the filter, and σ determines the velocity range that is filtered. 4 velocity filters were used, centered around velocities of 0, 5, 10, and 15 mm/s, with a value for σ of 10mm/s.

3) Localization: number of expected MBs: The number of expected MBs is the number of the brightest local maxima per frame, which are considered as potential MBs in the tracking algorithm.

4) Tracking: minimum track length and maximum linking distance: The minimum track length is a threshold for the minimum number of frames during which a potential MB has to be tracked. Structures that were tracked for a lower number of frames were rejected. The maximum linking distance is the distance a MB is allowed to travel between two frames to be considered as the same MB by the tracking algorithm.

H. Experiments

1) Embryo acquisitions: The chicken embryo in the modified weighing boat was placed on a heating plate which was set to 40°C. Before the acquisition, 70 μl of the SonoVue MBs suspension was injected intravenously under a stereomicroscope using a 0,3 ml syringe with a 29G needle. Before starting the acquisition, some saline was added on top of the embryo's CAM to enable ultrasound imaging of the CAM from the side (otherwise the vessels might be higher than the surroundings and would not be reachable by the ultrasound from the side). The acquisition duration was 10 seconds, which corresponds to 5000 compounded frames. The transmit voltage was set to 11V and the maximal imaging depth was 4 cm. The dependency of peak negative pressure on the transmit voltage can be seen in Supplementary Figure 12.

2) Rabbit Kidney acquisitions: The main artery of the rabbit kidney was connected to a hose through which the microbubble suspension was pumped (Supplementary Figure 8). The original MB suspension was diluted to obtain a concentration of $10^7 \frac{MB}{ml}$. The MB suspension was pumped through the kidney with a flow rate of 45ml/h. The acquisition duration was 30s, corresponding to 15000 compounded frames. The transmit voltage was set to 4V and the maximal imaging depth was 4 cm.

3) Phantom acquisitions: For imaging of the phantom, the initial SonoVue MB suspension was diluted 1000 fold resulting in a MB concentration of $2 * 10^5 \frac{MB}{ml}$. The diluted suspension was pumped through the two tubes of the phantom with a flow rate of 12 ml/h, corresponding to an average flow speed of approximately 100 mm/s. The crossing of the tubes was imaged under different angles ϑ to analyze the effects of the acquisition angle on the resolution. The ϑ = 0 angle was defined as when the bisector of the smaller angle between the tubes was parallel to the lateral direction of the transducer (Supplementary Figure 2). Acquisitions were made at three angles (approx. ϑ = 0°, ϑ = 20°, ϑ = 45°, the actual angle was determined in the analysis). Acquisitions under bigger angles for ϑ were not possible due to the phantom design. All acquisitions lasted 10 seconds, which corresponds to 5000 frames per acquisition. The transmit voltage was set to 20V and the maximal imaging depth was 12 cm. Parameters used for SRUS processing of acquisitions of the phantom can be found in Supplementary Table 1.

I. Simulations

Simulations were performed on the built-in Verasonics Simulations software. A field of view with moving point scatterers was simulated, where the trajectory of point scatterers was simulating laminar flow in the phantom. The average flow speed was 100 mm/s. In the first frame, 20 point-scatterers

were placed at random positions within the tubes. After a scatterer left a tube on one side, a new scatter appeared on the other side of the same tube so that the simulated MB concentration was constant. The same acquisition scripts as for the phantom acquisitions were used. Before SRUS processing, clutter noise modeled by Gaussian-filtered white Gaussian noise with a noise level of -20 dB was added to the simulations [7]. Simulations were performed under five angles (ϑ = 0°, ϑ = 25°, ϑ = 50°, ϑ = 75°, ϑ = 90°). Parameters used for SRUS processing of simulations of phantom acquisitions can be found in Supplementary Table 1.

J. Analysis and metrics

To analyze the effect of different processing parameters, acquisitions of the chicken embryo were compared in terms of the saturation of the SRUS image, the distribution of MB speeds, and the number and length of detected tracks. Furthermore, the SRUS images were visually inspected for the number of visible vessels and present noise in between vessels.

The angular dependence of SRUS imaging was analyzed by measuring the length of the region in which the two tubes were fully overlapping. The measured distance is further described in Supplementary materials and is called "overlap length" (Supplementary Figure 3). This measurement was done for all different angles and both B-Mode and SRUS images. The criterion of separation of the tubes was an intensity drop between the tubes to 10% of the maximum intensity in the tube. With a tube width of 200 μm and an angle of 30° between the tubes, the calculated overlap length was 0.7727 mm.

III. Results

A. Processing Parameters

Figure 1 shows the reference SRUS image of the CAM (Figure 1 A) and SRUS image of the CAM obtained by using different processing parameters (Figure 1 B-I). An evaluation of the same parameters (except for initial pixel size) on acquisitions of a rabbit kidney can be found in Supplementary Figure 11. Entire SRUS and power Doppler images of the chicken embryo and the rabbit kidney can be found in Supplementary Figures 7 and 10 respectively. On chicken embryo acquisitions the correlation across all frames compared to one frame at the center of the acquisition is 93% of the time higher than 0.97 (Supplementary Figure 6).

1) B-Mode image reconstruction: Initial pixel size: The Verasonics instructions suggest using the transducer element spacing as lateral pixel size for image reconstruction, since a smaller pixel size results in longer processing and is not necessary in most applications. Increasing the lateral pixel size from 0.5λ to the transducer spacing (1.4805λ) resulted in a decrease of resolution in lateral direction (Figure 1 B). Vessels that are close to each other in lateral direction are less resolved and start merging. Also, vessel walls are not as smooth and have little spikes in the lateral direction. When SRUS processing was performed on images that were reconstructed with a pixel size of 1.4805λ in lateral direction and then interpolated to square pixels of 0.5λ, the SRUS images showed some gridding in the lateral direction (Figure 1 C).

2) Filtering: SVD cutoff and additional filtering: The effect of the SVD cutoff value was evaluated and filtering setups for filtering MB by their velocity were compared. A higher SVD cutoff value led to the disappearance of small vessels on the SRUS image (Figure 1 D) as compared to the reference image. On the saturation curve, it can be seen that with a longer time not many more vessels would become visible. Filtering by MB velocity twice, once using an SVD and a Butterworth bandpass filter and once using only an SVD filter with a higher cutoff [10] resulted in an image with little noise and the appearance of more small vessels as compared to the reference image. On Figure 1 E) vessels have well-defined walls and vessels that are close to each other are well separated. The saturation curve with these processing parameters rised second highest without the introduction of much noise. When cone-shaped filters in Fourier space [9] were applied, more vessels became visible as compared to the reference, however, vessels that were close to each other merged. Furthermore when filtering for fast-moving MBs also many slow MB were detected indicating a limited filter performance (Figure 1 F MB speed distribution).

3) Localization: number of expected MBs: An increase of the number of expected MBs per frame resulted in an image on which more small vessels are seen (Figure 1 G). At the same time, noise appeared in between vessels.

4) Tracking: minimum track length and maximum linking distance: The maximum linking distance and minimum track length determine how far a MB may travel between subsequent frames and over how many frames a MB has to be tracked respectively. The histograms of the track lengths (Figure 1) show that the shorter the minimum track length, the more tracks were detected (the histogram is cut off at the minimum track length). When reducing the minimum track length, more vessels became visible, however, vessels in proximity were separated worse and the edges of vessels were getting less defined (Figure 1 H). If the maximum linking distance was increased, unrelated MBs were more often connected, which was especially observed at vessel branching sites (Figure 1 I).

B. Angular dependence

The effect of the flow orientation with respect to the transducer on SRUS images was tested on images of the crossed tubes flow phantom and simulations of that phantom. Figure 2 shows an example power Doppler and SRUS images of phantom acquisitions and simulations. SRUS image showed a higher resolution than power Doppler images.

1) Simulation: The flow orientation affected the resolution in power Doppler images of the simulated data (Figure 3). The bigger the angle of rotation ϑ of the tubes, the bigger the measured overlap length. On SRUS images no correlation between the angle of the tubes and the transducer can be seen. Nevertheless, close to the crossing of the two tubes, the tracking algorithm sometimes connected MBs from different tubes. This connection happened independently of ϑ.

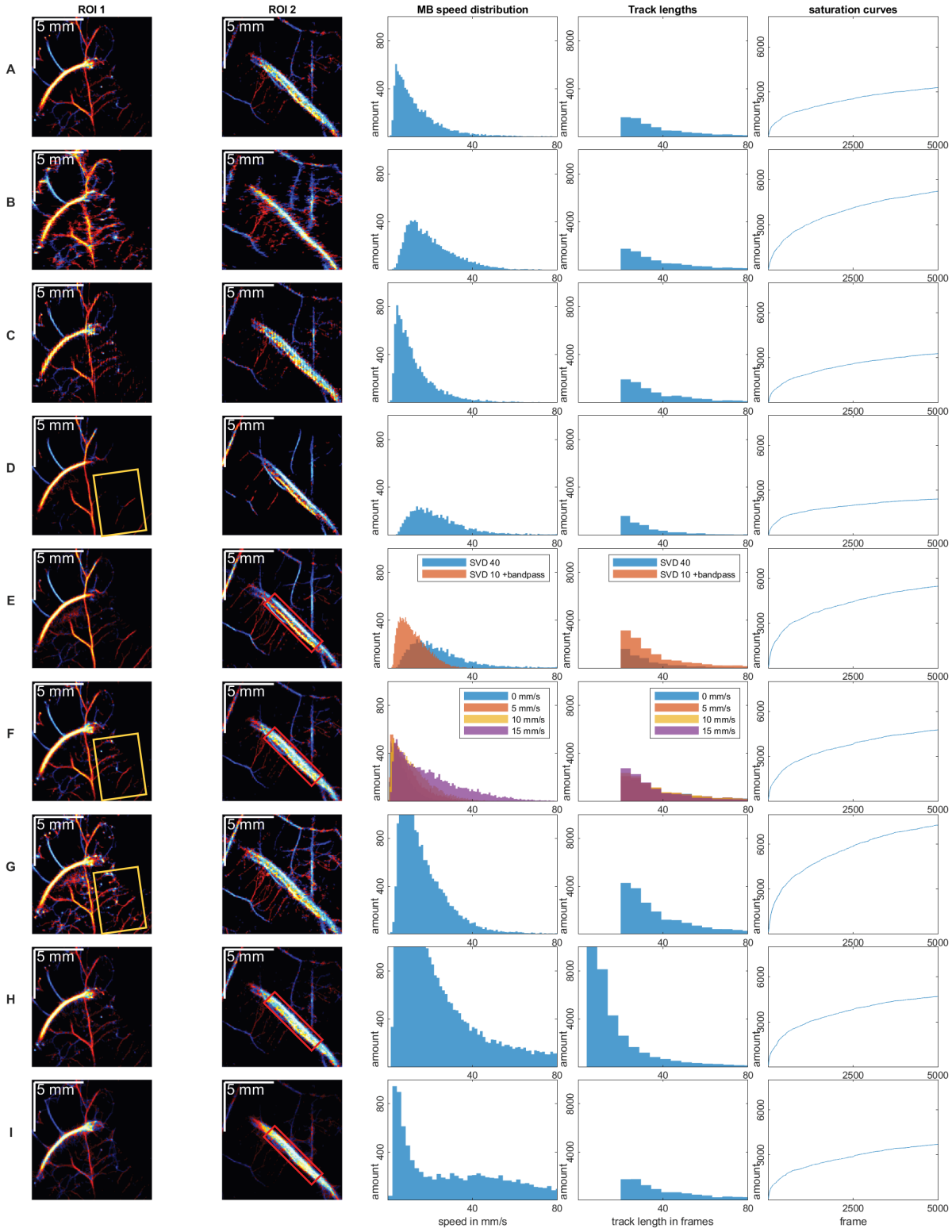

Fig. 1. Two regions of interest, histograms of MB speed, track length and image pixel saturation of SRUS images of the embryo's CAM vasculature. In the regions of interest red vessels have flow in upward direction and blue vessels have flow in downward direction. Yellow boxes indicate the appearance/disappearance of small vessels, red boxes show where close-by vessels were well/badly separated. For each row processing parameters were changed: A: the reference image, B: the pixel size for B-Mode reconstruction was set to 1.4805λ in lateral direction, C: the pixel size for B-Mode reconstruction was set to 1.4805λ in lateral direction and then the B-Mode image was interpolated to 0.5λ pixels, D: SVD cuff was set to 40, E: filter design as described in [10], F: filter design as described in [9], G: expected number of MBs was increased to 500, H: the minimal allowed track length was decreased to 7, I: the maximal allowed linking distance for the tracking algorithm was increased to 4 pixels.

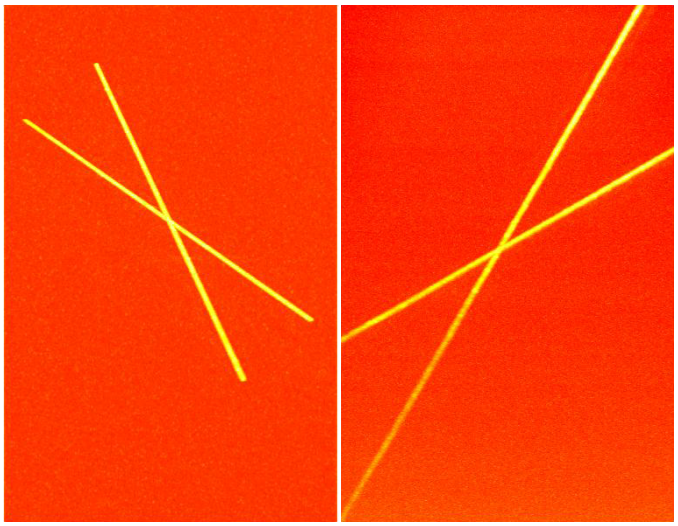

(a) (b)

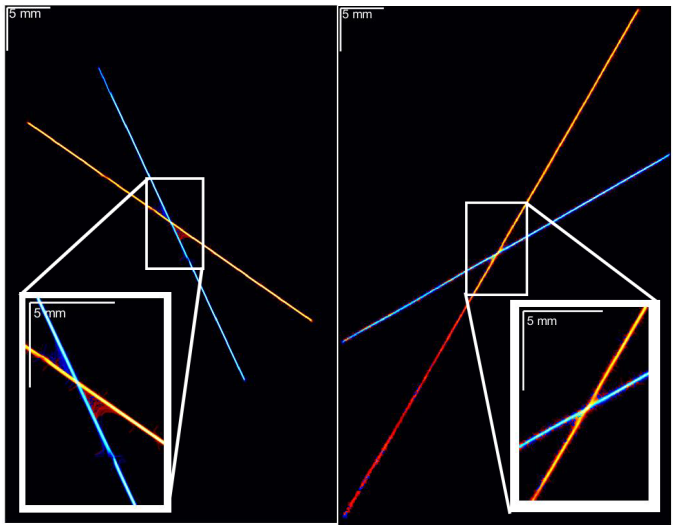

(c) (d)

Fig. 2. (a) power Doppler Simulation, (b) power Doppler phantom acquisition, (c) SRUS of Simulation, (d) SRUS of phantom acquisition

2) Acquisition: The observed angular dependency in power Doppler images on simulations cannot be seen in the acquisition data (Figure 3). The measured overlap length is inconsistent on power Doppler images without any visible tendency regarding ϑ. As in the simulations, the overlap length is consistent for SRUS images. While in Simulations the measured overlap length differed between B-Mode and SRUS images by a factor of 1,8 up to 2,3, the overlap length on power Doppler images of phantom acquisitions was only 1,3 to 1,6 times bigger than on SRUS images. On neither of the SRUS images the theoretical overlap length of 0.7727 mm was measured.

IV. Discussion

I have investigated the effect of different processing parameters of SRUS imaging. Other studies have focused on separate steps of SRUS processing, such as filtering [9] [11] [13],

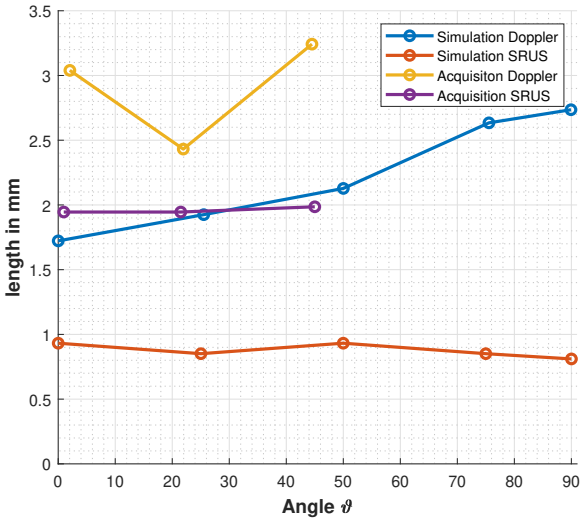

Fig. 3. Influence of flow direction on image resolution: The measured overlap length was plotted against the rotation angle ϑ of the phantom/simulation.

localization methods [7] [8] or tracking [14] [15]. I looked into parameters beginning from B-Mode image reconstruction until the tracking of MBs. In this work, I analyzed the effects of processing parameters (Table II) and I am proposing a guideline on how to adjust reconstruction parameters using an already reconstructed SRUS image of the same data or using knowledge of the acquisition (Table III).

The filtering step is probably the most crucial step in SRUS processing. Without filtering, MBs would not be visible because of tissue signal. SVD-based filters have been widely used in SRUS [1] [16] [17]. Different techniques were explored to improve the performance of SVD filters (adaptive SVD [18], noise equalization [11], block-wise SVD [13]). In general, tissue signal is concentrated in the low-order singular vectors, blood signal is concentrated in intermediate singular vectors and noise is concentrated in high-order singular vectors [11] [18]. Thus, setting the SVD cutoff too high results in the rejection of slow-moving MBs, since they resemble tissue signal. Setting the SVD cutoff too low does not suppress tissue enough. Huang et al. [9] proposed to separate MBs by their speed and their flow direction. This ensures less MBs per frame, simplifying detection and tracking. When MB localization is performed multiple times following the application of different filters, the same MB may be detected multiple times. These multiple detections can influence a qualitative analysis of MB counting or flow, however, they are acceptable for a qualitative image [9] [19]. This study confirms that filtering MBs by their speed allows the detection of small vessels without introduction of much noise. However, in this study only a split of MBs in two subgroups as proposed by Denis et al. [10] showed improvement with respect to the reference image. Huang et al. [9] went up to a 5 split of velocities. I tried to implement this algorithm, however, applying a cone-shaped filter in Fourier space resulted in a distorted MB appearance so that accurate MB localization was not possible. I assume that improving the filter design

TABLE II
EFFECTS OF PROCESSING PARAMETERS ON THE SRUS IMAGE

Parameter	too low/small	too high/big
pixel size in B-Mode reconstruction	Pixel sizes of smaller than 0.5λ were not tested, however, an improvement for SRUS imaging is not likely and image sizes rise quadratically with a linear decrease of pixel size in each direction.	Resolution loss in SRUS due to not exact localization. Song et al. presented a way on how to determine the minimum requirement for pixel size [8] .
number of expected MBs	Only a small number of MBs is detected and tracked which would result in long acquisitions. Furthermore, faster MBs appear brighter on SVD-filtered images due to their lower correlation on different frames, so only fast-moving MBs will be tracked.	Structures that are not MBs start appearing in the image resulting in artifacts or noise.
minimum track length	Structures that are not MBs start appearing in the image resulting in artifacts or noise. However, if the MB concentration is very high in the vessels a short minimum track length is beneficial, since MBs are overlapping often and are difficult to track.	Only a little number of MBs can be tracked for a long time
maximum linking distance	Fast moving MBs cannot be tracked.	MBs which are not related to each other start being connected by the tracking algorithm.

TABLE III
GUIDELINE FOR SETTING PROCESSING PARAMETERS FOR SRUS IMAGING

	filtering	expected number of MB	minimum track length	maximum linking distance	other reasons
little amount of vessels visible	filter suppresses not only tissue but also MB	too low; only brightest MB are detected	too high; MB cannot be tracked for a long enough time	too low; fast moving MB are not tracked	too low MB concentration in the acquisition or a too short acquisition
Tracks not well resolved	filtering can lead to distortion of MB			too high; MBs are linked to structures which are not in a vessel or in different vessels	too small pixels in B-Mode reconstruction, Song et al. describe a minimal requirement for the pixel size [8]
Noise between vessels		too high; structures that are not MB are considered as MB	too short; structures, that are not MB are considered as MB		
High MB concentration on acquisitons	beneficial to filter MB by velocity	beneficial to increase the expected number of MB per frame, since more MB per frame	beneficial to lower the track length since MB overlapping happens often		
low MB concentration on acquisitions		beneficial to decrease the expected number of MB per frame, since less MB per frame	can be set higher, since MB overlapping does happen less often		

would also improve the image quality. Furthermore, Huang et al. also split the data by flow direction (towards or away from the transducer). Implementing this split in my study might have improved MB detection, but would not have resolved MB distortion when performing a velocity split. The Fourier space filtering introduced by Huang et al. was taken further [19] [20], by using tilted planes instead of cones in Fourier spaces. Along these planes, MB signals of a certain velocity and direction are concentrated. Dencks et al. [19] applied a filter in 8 different directions for three different velocities. Applying such directional filters could also prevent some tracking errors.

It is difficult to track MBs correctly in close-by vessels. This was seen on embryo acquisitions, where close-by vessels sometimes started merging, as well as on acquisitions of the phantom, where tracks close to the crossing ”jumped” from one tube to the other. The probability of wrong pairing rises particularly with comparably high MB concentrations. Applying the directional filters described in the previous paragraph might prevent tracking errors of MB in close-by vessels with different flow directions. Other ways to reduce tracking errors are more advanced tracking algorithms that take into account surrounding flow or the previous MB location. In this study, the nearest neighbor approach was used for tracking, due to its simplicity and the present implementation [7] [10]. Kalman tracking is another widely used algorithm, which outperforms nearest neighbor based tracking algorithms SRUS [21] [14] [22] [23]. Assumptions, such as constant velocity or accelerated movement can be implemented in the cost function of Kalman filter based tracking algorithms [23].

The theoretical resolution limit in SRUS was described by Desailly et al. [6]. Practically the resolution of SRUS images was measured by Hingot et al. [5] using the Fourier Ring Correlation (FRC). Song et al. [8] and Heiles et al. [7] measured the localization accuracy of single MBs. In their

studies, the localization of a single MB was more accurate in lateral than in axial direction [7], especially with big pixel sizes in B-Mode images [8]. This might be counterintuitive since lateral resolution is lower than axial resolution in B-Mode ultrasound imaging. However, due to the lower resolution in lateral direction in B-Mode images, the profile of the PSF of a MB in lateral direction is wider than in axial direction. This leads to more spatial samples per microbubble, which indicate the MB's actual position. Thus, the lower lateral resolution compared to the axial resolution of B-Mode imaging might, to some extent, lead to a higher lateral than axial resolution in SRUS imaging. In the publication by Hingot et al. [5] this effect is slightly visible in the directional analysis of FRC. In my study acquisitons of the crossed tubes phantom did not show any directional dependence of the resolution. I assume that this is due to a too-high MB concentration in phantom acquisitions which made precise detection and tracking of MB difficult. A longer acquisition with a lower MB concentration might provide a better SRUS image. Furthermore, acquisitions on a smaller phantom resulting in a lower imaging depth and therefore in a lower noise level as well as a higher initial resolution might give more meaningful results.

A. Limitations and outlook

I have shown how different parameters influence the quality of SRUS images, as well as the effect of different flow directions on these images. Parameters that have to be set for SRUS processing depend on the processing pipeline. Due to the accessibility of the code by Denis et al., I decided to give an overview of the parameters used in their implementation.

The simulations performed for this study were simplified as compared to reality. Laminar flow was approximated by 10 discrete velocities over the cross-section of the tubes. Furthermore, the simulations were performed without any additional scatterers, and noise was added after the reconstruction of the IQ data. For this study, these limitations were assumed to not influence the results. For resolution measurements, simulations and the crossed tubes phantom was used. In a future study, the angle between the tubes should be reduced in such a phantom, to get more accurate results. Having a smaller angle would increase the region of interest, where the tubes are close to each other and difficult to separate. Heiles et al. [7] simulated two diverging tubes that had a maximal distance of 1λ, which allows a precise measurement of where the tubes cannot be separated anymore.

On the chicken embryo acquisitions in this study, no motion compensation was applied. This was possible because of very little movement during the acquisition, however, for other *in vivo* acquisitions, motion compensation algorithms should be applied.

V. Conclusion

In this study, an overview of a selection of parameters for SRUS imaging was given and the effect of flow direction on SRUS images was analyzed. A guideline was established on how to choose the correct processing parameters depending on visual image artifacts and knowledge about the acquired data. From visual inspection, image filtering had the biggest effect on SRUS images. It was also found that while flow orientation affects the resolution of conventional US images no effect of flow orientation on the SRUS images was found.

VI. Laymen's Summary

About 130 years ago it was impossible to see inside the human body without cutting it open. In 1895, the German scientist Wilhelm Conrad Röntgen discovered X-ray radiation, which for the first time allowed imaging of bones inside a living human. During the last century, many other imaging modalities were developed and are now widely used in healthcare. Whether for diagnosis of fractured bones, tumor detection, or checkups during pregnancy - different medical imaging modalities are used. One remaining challenge is to obtain high-resolution images from deep within the human body. For instance, imaging of very small blood vessels can reveal information about diseases or lesions. Super Resolution Ultrasound Imaging tackles the problem of obtaining high-resolution images of small blood vessels that are located deep inside the body. To get a good image, a lot of parameters have to be set correctly. In the given study, the effect of a selection of these parameters was examined. Another question was on how much it matters from what direction blood vessels are imaged. This should give more understanding of how to obtain high-quality images, which might help in the diagnosis of certain diseases in the future.

References

[1] P. Song, J. M. Rubin, and M. R. Lowerison, "Super-resolution ultrasound microvascular imaging: Is it ready for clinical use?" *Zeitschrift für Medizinische Physik*, May 2023. [Online]. Available: https://www.sciencedirect.com/science/article/pii/S0939388923000430

[2] E. Abbe, "Beiträge zur Theorie des Mikroskops und der mikroskopischen Wahrnehmung," *Archiv für Mikroskopische Anatomie*, vol. 9, no. 1, pp. 413–468, Dec. 1873. [Online]. Available: https://doi.org/10.1007/BF02956173

[3] "The Nobel Prize in Chemistry 2014." [Online]. Available: https://www.nobelprize.org/prizes/chemistry/2014/press-release/

[4] C. Errico, J. Pierre, S. Pezet, Y. Desailly, Z. Lenkei, O. Couture, and M. Tanter, "Ultrafast ultrasound localization microscopy for deep super-resolution vascular imaging," *Nature*, vol. 527, no. 7579, pp. 499–502, Nov. 2015, number: 7579 Publisher: Nature Publishing Group. [Online]. Available: https://www.nature.com/articles/nature16066

[5] V. Hingot, A. Chavignon, B. Heiles, and O. Couture, "Measuring Image Resolution in Ultrasound Localization Microscopy," *IEEE Transactions on Medical Imaging*, vol. 40, no. 12, pp. 3812–3819, Dec. 2021, conference Name: IEEE Transactions on Medical Imaging. [Online]. Available: https://ieeexplore.ieee.org/document/9490980

[6] Y. Desailly, J. Pierre, O. Couture, and M. Tanter, "Resolution limits of ultrafast ultrasound localization microscopy," *Physics in Medicine and Biology*, vol. 60, no. 22, pp. 8723–8740, Nov. 2015. [Online]. Available: https://iopscience.iop.org/article/10.1088/0031-9155/60/22/8723

[7] B. Heiles, A. Chavignon, V. Hingot, P. Lopez, E. Teston, and O. Couture, "Performance benchmarking of microbubble-localization algorithms for ultrasound localization microscopy," *Nature Biomedical Engineering*, vol. 6, no. 5, pp. 605–616, May 2022, number: 5 Publisher: Nature Publishing Group. [Online]. Available: https://www.nature.com/articles/s41551-021-00824-8

[8] P. Song, A. Manduca, J. D. Trzasko, R. E. Daigle, and S. Chen, "On the Effects of Spatial Sampling Quantization in Super-Resolution Ultrasound Microvessel Imaging," *IEEE Transactions on Ultrasonics, Ferroelectrics, and Frequency Control*, vol. 65, no. 12, pp. 2264–2276, Dec. 2018, conference Name: IEEE Transactions on Ultrasonics, Ferroelectrics, and Frequency Control. [Online]. Available: https://ieeexplore.ieee.org/document/8354905

[9] C. Huang, M. R. Lowerison, J. D. Trzasko, A. Manduca, Y. Bresler, S. Tang, P. Gong, U.-W. Lok, P. Song, and S. Chen, "Short Acquisition Time Super-Resolution Ultrasound Microvessel Imaging via Microbubble Separation," *Scientific Reports*, vol. 10, no. 1, p. 6007, Apr. 2020. [Online]. Available: https://www.nature.com/articles/s41598-020-62898-9

[10] L. Denis, S. Bodard, V. Hingot, A. Chavignon, J. Battaglia, G. Renault, F. Lager, A. Aissani, O. Hélénon, J.-M. Correas, and O. Couture, "Sensing ultrasound localization microscopy for the visualization of glomeruli in living rats and humans," *eBioMedicine*, vol. 91, p. 104578, May 2023. [Online]. Available: https://www.sciencedirect.com/science/article/pii/S2352396423001433

[11] P. Song, A. Manduca, J. D. Trzasko, and S. Chen, "Noise Equalization for Ultrafast Plane Wave Microvessel Imaging," *IEEE Transactions on Ultrasonics, Ferroelectrics, and Frequency Control*, vol. 64, no. 11, pp. 1776–1781, Nov. 2017, conference Name: IEEE Transactions on Ultrasonics, Ferroelectrics, and Frequency Control. [Online]. Available: https://ieeexplore.ieee.org/document/8024013

[12] R. Parthasarathy, "Rapid, accurate particle tracking by calculation of radial symmetry centers," *Nature Methods*, vol. 9, no. 7, pp. 724–726, Jul. 2012, number: 7 Publisher: Nature Publishing Group. [Online]. Available: https://www.nature.com/articles/nmeth.2071

[13] P. Song, A. Manduca, J. D. Trzasko, and S. Chen, "Ultrasound Small Vessel Imaging With Block-Wise Adaptive Local Clutter Filtering," *IEEE Transactions on Medical Imaging*, vol. 36, no. 1, pp. 251–262, Jan. 2017, conference Name: IEEE Transactions on Medical Imaging. [Online]. Available: https://ieeexplore.ieee.org/document/7559732

[14] J. Yan, T. Zhang, J. Broughton-Venner, P. Huang, and M.-X. Tang, "Super-Resolution Ultrasound Through Sparsity-Based Deconvolution and Multi-Feature Tracking," *IEEE Transactions on Medical Imaging*, vol. 41, no. 8, pp. 1938–1947, Aug. 2022, conference Name: IEEE Transactions on Medical Imaging.

[15] T. Lisson, J. Salewski, S. Dencks, and G. Schmitz, "Resolution Improvement of ULM Images Applying a Rauch-Tung-Striebel Smoother," in *2023 IEEE International Ultrasonics Symposium (IUS)*, Sep. 2023, pp. 1–4, iSSN: 1948-5727. [Online]. Available: https://ieeexplore.ieee.org/document/10306605

[16] K. Christensen-Jeffries, O. Couture, P. A. Dayton, Y. C. Eldar, K. Hynynen, F. Kiessling, M. O'Reilly, G. F. Pinton, G. Schmitz, M.-X. Tang, M. Tanter, and R. J. G. van Sloun, "Super-resolution Ultrasound Imaging," *Ultrasound in Medicine & Biology*, vol. 46, no. 4, pp. 865–891, Apr. 2020. [Online]. Available: https://www.sciencedirect.com/science/article/pii/S0301562919315959

[17] O. Couture, V. Hingot, B. Heiles, P. Muleki-Seya, and M. Tanter, "Ultrasound Localization Microscopy and Super-Resolution: A State of the Art," *IEEE Transactions on Ultrasonics, Ferroelectrics, and Frequency Control*, vol. 65, no. 8, pp. 1304–1320, Aug. 2018, conference Name: IEEE Transactions on Ultrasonics, Ferroelectrics, and Frequency Control.

[18] J. Baranger, B. Arnal, F. Perren, O. Baud, M. Tanter, and C. Demené, "Adaptive Spatiotemporal SVD Clutter Filtering for Ultrafast Doppler Imaging Using Similarity of Spatial Singular Vectors," *IEEE Transactions on Medical Imaging*, vol. 37, no. 7, pp. 1574–1586, Jul. 2018, conference Name: IEEE Transactions on Medical Imaging. [Online]. Available: https://ieeexplore.ieee.org/document/8281060

[19] S. Dencks, M. Piepenbrock, and G. Schmitz, "Velocity Filtering with a Median Filter Better Preserves Small Vessels for Ultrasound Localization Microscopy," in *2021 IEEE International Ultrasonics Symposium (IUS)*, Sep. 2021, pp. 1–4, iSSN: 1948-5727. [Online]. Available: https://ieeexplore.ieee.org/document/9593882

[20] U. Soylu and Y. Bresler, "Circumventing the resolution-time tradeoff in Ultrasound Localization Microscopy by Velocity Filtering," Jan. 2021, arXiv:2101.09470 [eess]. [Online]. Available: http://arxiv.org/abs/2101.09470

[21] C. Huang, W. Zhang, P. Gong, U.-W. Lok, S. Tang, T. Yin, X. Zhang, L. Zhu, M. Sang, P. Song, R. Zheng, and S. Chen, "Super-resolution ultrasound localization microscopy based on a high frame-rate clinical ultrasound scanner: an in-human feasibility study," *Physics in Medicine & Biology*, vol. 66, no. 8, p. 08NT01, Apr. 2021, publisher: IOP Publishing. [Online]. Available: https://dx.doi.org/10.1088/1361-6560/abef45

[22] I. Taghavi, S. B. Andersen, C. A. V. Hoyos, M. Schou, F. Gran, K. L. Hansen, M. B. Nielsen, C. M. Sørensen, M. B. Stuart, and J. A. Jensen, "Ultrasound super-resolution imaging with a hierarchical Kalman tracker," *Ultrasonics*, vol. 122, p. 106695, May 2022. [Online]. Available: https://www.sciencedirect.com/science/article/pii/S0041624X22000105

[23] B. Huang, J. Yan, M. Morris, V. Sinnett, N. Somaiah, and M.-X. Tang, "Acceleration-Based Kalman Tracking for Super-Resolution Ultrasound Imaging In Vivo," *IEEE Transactions on Ultrasonics, Ferroelectrics, and Frequency Control*, vol. 70, no. 12, pp. 1739–1748, Dec. 2023, conference Name: IEEE Transactions on Ultrasonics, Ferroelectrics, and Frequency Control. [Online]. Available: https://ieeexplore.ieee.org/document/10292714